


Available online at www.sciencedirect.com
ScienceDirect
Procedia IUTAM 16 (2015) 3 – 11
Procedia IUTAM
www.elsevier.com/locate/procedia

IUTAM Symposium on Dynamics of Capsules, Vesicles and Cells in Flow

Rheological properties of sheared vesicle and cell suspensions

Antonio Lamura[a,*], Gerhard Gompper[b]

[a]*Istituto Applicazioni Calcolo, CNR, Via Amendola 122/D, 70126 Bari, Italy*
[b]*Theoretical Soft Matter and Biophysics, Institute of Complex Systems, Forschungszentrum Jülich, 52428 Jülich, Germany*

Abstract

Numerical simulations of vesicle suspensions are performed in two dimensions to study their dynamical and rheological properties. An hybrid method is adopted, which combines a mesoscopic approach for the solvent with a curvature-elasticity model for the membrane. Shear flow is induced by two counter-sliding parallel walls, which generate a linear flow profile. The flow behavior is studied for various vesicle concentrations and viscosity ratios between the internal and the external fluid. Both the intrinsic viscosity and the thickness of depletion layers near the walls are found to increase with increasing viscosity ratio.

Peer-review under the responsibility of the organizing committee of DYNACAPS 2014 (Dynamics of Capsules, Vesicles and Cells in Flow).

Keywords: Vesicles, Rheology, Shear flow, Numerical modeling

1. Introduction

A detailed understanding of the dynamical and rheological properties of suspensions of vesicles, cells, and capsules is relevant for a wide range of applications, ranging from soft glasses to blood flow.[1,2,3] Vesicles are deformable particles made by a closed lipidic membrane encapsulating a fluid whose rheology strongly depends on the bending of the membrane, on the viscosity contrast (the ratio of the viscosity η_{in} of the embedded fluid to that η_{out} of the surrounding fluid), and on the concentration. The goal of experimental, theoretical and simulation studies is to obtain a complete picture of vesicle dynamics under flow. Moreover, vesicles can be considered as a model for more complex systems such as red blood cells. Here, the main difference between vesicles and red blood cells is that the latter have a cytoskeleton attached to the lipid bilayer which implies a shear modulus of the composite membrane.

In dilute systems, vesicles show tank-treading (TT), tumbling (TU), and vacillating-breathing motion[1] depending on shear rate and viscosity contrast $\lambda = \eta_{in}/\eta_{out}$. In the case of a highly dilute suspension of quasi-spherical vesicles, it has been predicted[4,5] that the intrinsic viscosity $\eta_I = (\eta - \eta_{out})/(\eta_{out}\phi)$, where η is the effective suspension viscosity and ϕ the vesicle concentration, decreases in the TT phase when λ increases, attains a minimum at the critical value $\lambda \simeq \lambda_c$ where there is the TT-to-TU transition, and then increases when $\lambda > \lambda_c$. This result has been checked both numerically and experimentally. While a number of simulations[6,7,8,9,10] and one experiment[11] confirmed this picture,

* Corresponding author. Tel.: +39-0805929745 ; fax: +39-0805929770.
E-mail address: a.lamura@ba.iac.cnr.it

Peer-review under the responsibility of the organizing committee of DYNACAPS 2014 (Dynamics of Capsules, Vesicles and Cells in Flow).
doi:10.1016/j.piutam.2015.03.002

another experimental study [12] and our recent numerical work [13] find the intrinsic viscosity to increase monotonically with increasing viscosity contrast.

In this paper, we will give an overview of the numerical results obtained on the basis of a two-dimensional vesicle model, which is characterized by the presence of thermal membrane undulations as well as of thermal noise which implies translational Brownian motion [13]. Both these features are missing in the other numerical approaches. We will briefly discuss their role in the obtained results for η_I, which will be given for different values of viscosity contrast, vesicle concentration, and swelling degree. Finally, the presence of depletion layers (or vesicle-free layers) near walls, in the case of concentrated suspensions, will be pointed out as a function of the viscosity contrast.

2. Model and Methods

In this section, we outline the model and mesoscale hydrodynamics approach employed in the simulations.

2.1. Solvent

We consider a two-dimensional fluid consisting of N point-like particles of mass m with positions $\mathbf{r}_i(t)$ and velocities $\mathbf{v}_i(t)$ at time t ($i = 1, 2, ..., N$) both of which are continuous variables. The present method is referred to as multi-particle collision dynamics [14,15,16], but it also known as stochastic rotation dynamics [17,18]. The evolution occurs in subsequent steps of propagation and collision. The streaming of particles is performed by moving them ballistically

$$\mathbf{r}_i(t + \Delta t) = \mathbf{r}_i(t) + \mathbf{v}_i(t)\Delta t \qquad i = 1, ..., N \tag{1}$$

with Δt the time between two collisions. For the scattering, the system is divided into the cells of a regular square lattice of mesh size a. Each of these cells is the interaction area where an instantaneous multi-particle collision occurs. In this step velocities are updated [19,20] as

$$\mathbf{v}_i^{new} = \mathbf{v}_c^G + \mathbf{v}_i^{ran} - \sum_{j \in cell} \mathbf{v}_j^{ran}/N_c + \mathbf{\Pi}^{-1} \sum_{j \in cell} m \left[\mathbf{r}_{j,c} \times (\mathbf{v}_j - \mathbf{v}_j^{ran})\right] \times \mathbf{r}_{i,c} \qquad i = 1, ..., N \tag{2}$$

where $\mathbf{v}_c^G$ is the velocity of the center of mass of all particles in the cell, $\mathbf{v}_i^{ran}$ is a velocity chosen from a Maxwell-Boltzmann distribution, N_c is the number of particles in the cell, $\mathbf{\Pi}$ is the moment-of-inertia tensor of the particles in the cell, and $\mathbf{r}_{i,c}$ is the position relative to the center of mass of the particles in the cell. The local linear and angular momenta are conserved under this dynamics [19,20] and the temperature is kept constant [21].

The viscosity of the fluid is given by [22]

$$\eta = \frac{m}{\Delta t}\left[\left(\frac{l}{a}\right)^2 \left(\frac{n^2}{n-1} - \frac{n}{2}\right) + \frac{1}{24}\left(n - \frac{7}{5}\right)\right] \tag{3}$$

with n the average number of particles per cell, $l = \Delta t \sqrt{k_B T/m}$ the mean-free path, and $k_B T$ the thermal energy. The viscosity η is the sum of a kinetic contribution η_{kin} due to particle streaming (the first term in the square brackets), and a collisional contribution η_{coll} due to particle scattering (the second term). Theory slightly underestimates η_{kin} and slightly overestimates η_{coll}. [22] At small values of the mean free path l/a, as in our case, η_{kin} is negligible and η_{coll} is a little larger than the numerical value. Due to this, the effective value of the fluid viscosity is numerically evaluated by measuring the xy component of the stress tensor σ_{xy} in a sheared system so that $\eta = \sigma_{xy}/\dot{\gamma}$ where $\dot{\gamma}$ is the shear rate. [23]

The system of size $L_x \times L_y$ is confined by two horizontal walls which slide along the x direction with velocities $\pm v_{wall}$. Periodic boundary conditions are used along the x direction. Bounce-back boundary conditions with virtual particles in partly filled cells are adopted to implement no-slip at the walls [24]. A linear flow profile $(v_x, v_y) = (\dot{\gamma} y, 0)$ is obtained with shear rate $\dot{\gamma} = 2v_{wall}/L_y$.

2.2. Vesicles

Each vesicle in two dimensions is modeled as a closed chain made of N_v beads of mass m_v connected successively.[25] The internal potential U is the sum of three contributions. The bending potential is

$$U_{bend} = \frac{\kappa}{r_0} \sum_{i=1}^{N_v} (1 - \cos\beta_i), \tag{4}$$

where κ is the bending rigidity, r_0 is the average bond length, and β_i is the angle between two successive bonds, which controls shapes and fluctuations. In order to keep the length of the membrane conserved, both locally and globally, the neighboring beads are connected to each other by the harmonic potential

$$U_{bond} = \kappa_h \sum_{i=1}^{N_v} \frac{(|\mathbf{r}_i - \mathbf{r}_{i-1}| - r_0)^2}{2r_0^2} \tag{5}$$

where κ_h is the spring constant and $\mathbf{r}_i$ is the position vector of the i-th bead. The constraint potential

$$U_{area} = \kappa_A \frac{(A - A_0)^2}{2r_0^4}, \tag{6}$$

where κ_A is the compression modulus and A_0 is the target area of the vesicle, is introduced to keep the internal area A of the vesicle constant.

Finally, different vesicles interact via a shifted repulsive Lennard-Jones potential

$$U_{rep} = 4\epsilon\left[\left(\frac{\sigma}{r}\right)^{12} - \left(\frac{\sigma}{r}\right)^{6}\right] + \epsilon \tag{7}$$

truncated at its minimum r_{cut}. Newton's equations of motions for the beads are integrated by using the velocity-Verlet algorithm with time step Δt_v.[26]

2.3. Solvent-Vesicle Coupling

Each bead is represented by a "rough" hard disk of radius r_v. The value of r_v is set in order to ensure overlap of disks and a full covering up of the membrane. Scattering occurs only when a solvent particle i and a disk j overlap and move towards each other so that the conditions $|\mathbf{r}_j - \mathbf{r}_i| < r_v$ and $(\mathbf{r}_j - \mathbf{r}_i)\cdot(\mathbf{v}_j - \mathbf{v}_i) < 0$ are both satisfied. A second disk $k = j \pm 1$, adjacent to the j-th one in the same membrane, with the smallest distance from the solvent particle i, is then selected. The center of mass velocity $\mathbf{v}^G$ and the angular velocity

$$\omega = \mathbf{\Pi}^{-1} \sum_{l=i,j,k} m_l \mathbf{r}_{l,c} \times \mathbf{v}_l \tag{8}$$

of the i, j, k-particle system are computed with $\mathbf{\Pi}$ the moment-of-inertia tensor and $\mathbf{r}_{l,c}$ the position relative to the center of mass. Their velocities are updated according to the rule

$$\mathbf{v}_l^{new} = 2(\mathbf{v}^G + \omega \times \mathbf{r}_{l,c}) - \mathbf{v}_l \qquad l = i, j, k \tag{9}$$

which ensures linear and angular momenta conservation.[27]

The collision step (2) is then executed only for the fluid particles which did not scatter with the membrane in order to prevent multiple collisions with the same disk in the following time steps. Membrane disks interact with walls also by bounce-back scattering.

2.4. Parameters

Experimental realizations of vesicle suspensions in shear flow are characterized by small values of the Reynolds number $Re = \dot{\gamma}\rho R_0^2/\eta_{out}$, with $\rho = nm/a^2$ the mass density. It is useful to express results in terms of dimensionless

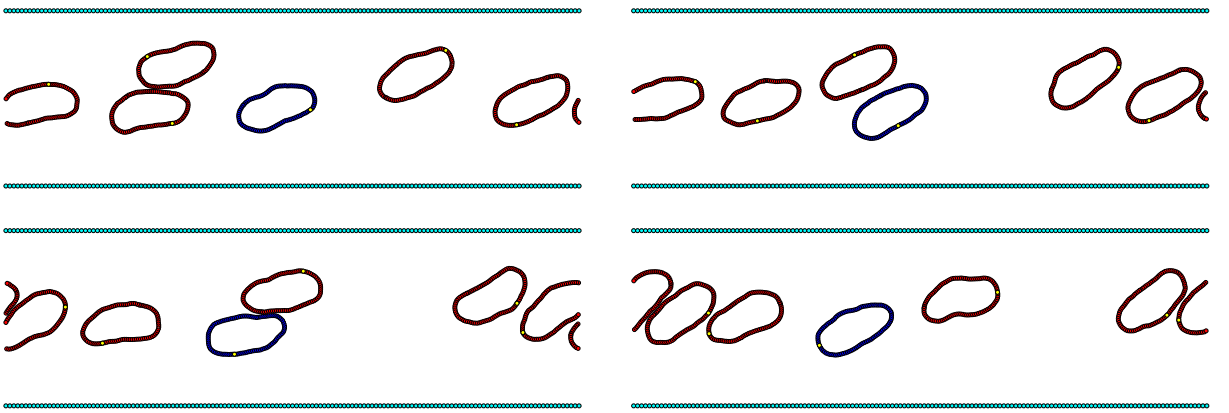

Fig. 1. Subsequent snapshots (from left to right, from top to bottom) at times $\dot{\gamma}t = 224, 226, 228, 230$ of vesicle conformations in shear flow with reduced shear rate $\gamma^* = 2.0$, reduced area $A^* = 0.8$, viscosity contrast $\lambda = 1.0$, and concentration $\phi = 0.14$. One vesicle is in blue for better visualization and the yellow bead indicates the tank-treading motion.

quantities such as the reduced area $A^* = A_0/\pi R_0^2$, where $R_0 = L_0/2\pi$ is the mean vesicle radius and L_0 is the membrane length, and the reduced shear rate (or capillary number) $\gamma^* = \dot{\gamma}\eta_{out}R_0^3/\kappa$. We set $n = 10$, $l_{out} = 0.0064a$ with $l_{in} = l_{out}\sqrt{m_{out}/m_{in}}$ (in the following the subscripts out/in will refer to quantities outside/inside the vesicle) so that the viscosity contrast is $\lambda = \eta_{in}/\eta_{out} \simeq m_{in}/m_{out}$. We use $L_x \times L_y = (18.95 \times 5.79)R_0$, $R_0 = 7.6a$, and v_{wall} such that $Re < 0.2$. Finally, m_{in} is set to have $0.1 \leq \lambda \leq 13.0$, $m_V = 3m_{out}$, $N_v = 480$, $\Delta t_v = \Delta t/64$, $r_v = r_0 = a/10$, $r_{cut} = a$, $\kappa = 6.58k_BTR_0$, $\kappa_A = 4 \times 10^{-4}k_BT$, $\kappa_h = 3 \times 10^2 k_BT$, $\epsilon = 10k_BT$, and A_0 in such a way that $A^* = 0.8, 0.95$.

3. Results

3.1. Suspension Viscosity

Dilute and semi-dilute monodisperse suspensions of vesicles are first considered with reduced shear rate $\gamma^* = 2.0$. This value of γ^* is comparable to those used in previous studies on vesicle rheology[6,8,9,10]. The suspension viscosity η is computed by measuring the xy component of the stress tensor σ_{xy} as $\eta = \sigma_{xy}/\dot{\gamma}$.[23]

Figure 1 shows a few typical snapshots of vesicles in shear flow. Vesicles displaced relative to each other in the shear-gradient direction move with different velocities and can therefore collide with each other. In the TT regime, vesicles generally move with a constant inclination angle; however, during a collision, they hug each other, which leads to a characteristic decrease and subsequent recovery of the inclination angle.[13]

The relative viscosity $(\eta - \eta_{out})/\eta_{out}$, displayed in Fig. 2, is a linear function of the concentration ϕ for reduced area $A^* = 0.8$ and different values of the viscosity contrast λ, in agreement with the linear dependence predicted by the Einstein relation for disks in two dimensions.[28] In Fig. 3, the intrinsic viscosity η_I is plotted as a function of λ for different concentrations with $A^* = 0.8$. In all the cases η_I is observed to increase in the explored range of viscosity contrast.[13] This is at odds with some numerical results[6,7,8,9,10] and one experiment,[11] where η_I decreases with λ, reaching a minimum at the TT-to-TU transition, and then increases in the tumbling regime, as theoretically predicted for a quasi-spherical vesicle in three dimensions.[4,5] In our simulations, we observe the transition from TT to TU with increasing λ. For the simulated value of $A^* = 0.8$, the Keller-Skalak (KS) theory[29] indicates the TT-to-TU transition to occur at $\lambda_c \simeq 3.7$. However, no evidence is found for the predicted dip in the intrinsic viscosity. We believe that this discrepancy can be traced back to the fact that our model includes thermal vesicle fluctuations, neglected in the KS theory, which are known to produce a continuous crossover from TT to TU.[27] Our results are consistent with other experimental results for semi-dilute vesicle suspensions.[12]

Also the case of a single quasi-circular ($A^* = 0.95$) vesicle is investigated, corresponding to concentration $\phi = 0.03$. As for the more deflated vesicle ($A^* = 0.8$) discussed above, after an initial transient the vesicle moves along the

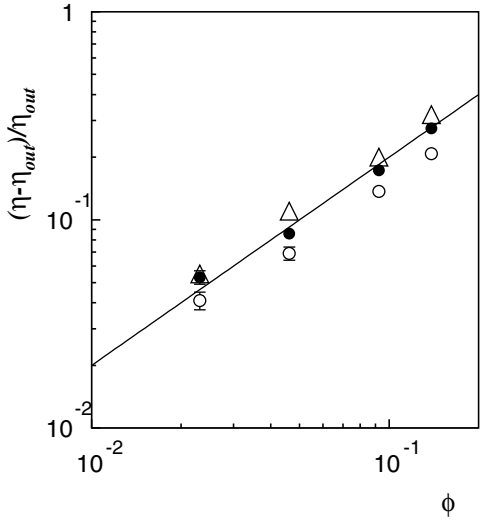

Fig. 2. The quantity $(\eta - \eta_{out})/\eta_{out}$ as a function of the concentration ϕ for reduced shear rate $\gamma^* = 2.0$, reduced area $A^* = 0.8$, and viscosity contrasts $\lambda = 1.0(\circ), 5.0(\bullet), 9.0(\triangle)$. The continuous line corresponds to the Einstein law $(\eta - \eta_{out})/\eta_{out} = 2\phi$ for disks in two dimensions.[28] When not visible, errors bars are comparable with symbols size.

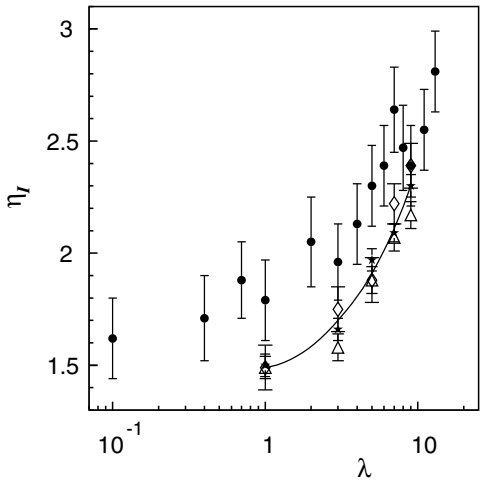

Fig. 3. The intrinsic viscosity $\eta_I = (\eta - \eta_{out})/(\eta_{out}\phi)$ as a function of the viscosity contrast λ for reduced shear rate $\gamma^* = 2.0$, reduced area $A^* = 0.8$, and concentration $\phi = 0.02(\bullet), 0.05(\diamond), 0.09(\triangle), 0.14(\star)$. The full line is the interpolations to the data for $\phi = 0.14$ $(\star)$. The tank-treading-to-tumbling transition occurs at $\lambda_c \simeq 3.7$ for $A^* = 0.8$ in the KS theory.

channel while diffusing laterally up to the longest simulated times $\sim 10^2/\dot{\gamma}$. The results for η_I are reported in Fig. 4 and confirm the general picture of intrinsic viscosity increasing with λ.

3.2. Depletion Layer

The effect of wall confinement is investigated for monodisperse concentrated suspensions with concentration $\phi = 0.28$, reduced area $A^* = 0.8$, and reduced shear rate $\gamma^* = 2.0$. It is well known[27] that the lift force induced by the hydrodynamic interaction of vesicles with nearby walls produces a depletion layer near the walls, as first observed for red blood cells in capillary flow.[30] We have measured the average thickness δ of such vesicle-free layers (also denoted cell-free layers in analogy with the case of red blood cells). Here, δ is defined as the time average of $(d_1(t) + d_2(t))/2$ where $d_1(t)$ and $d_2(t)$ are the distances at time t of the two vesicle beads closest to the two walls, respectively. The

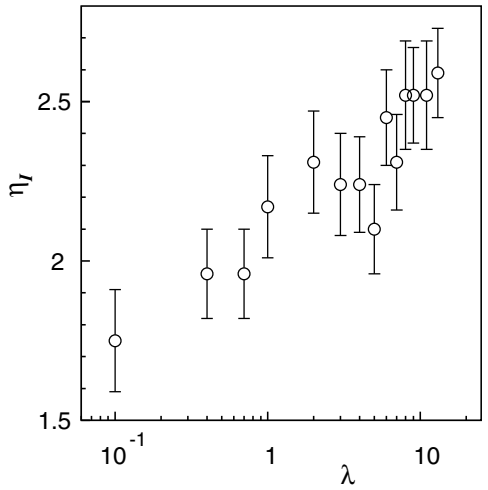

Fig. 4. The intrinsic viscosity $\eta_I = (\eta - \eta_{out})/(\eta_{out}\phi)$ as a function of the viscosity contrast λ for reduced shear rate $\gamma^* = 2.0$, reduced area $A^* = 0.95$, and concentration $\phi = 0.03$. The tank-treading-to-tumbling transition occurs at $\lambda_c \simeq 6.5$ for $A^* = 0.95$ in the KS theory.

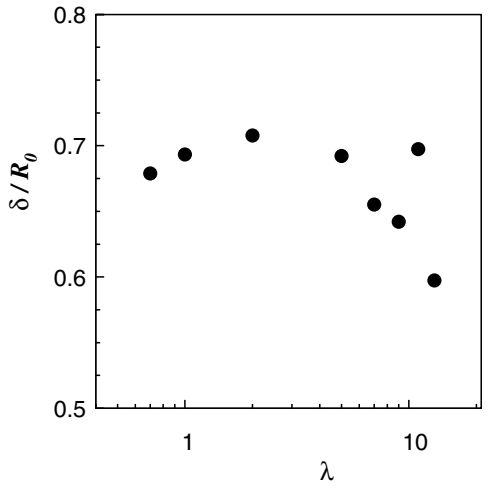

Fig. 5. The average cell-free boundary layer δ as a function of the viscosity contrast λ for reduced shear rate $\gamma^* = 2.0$, reduced area $A^* = 0.8$, and concentration $\phi = 0.28$. Error bars are comparable with symbols size.

behavior of δ as a function of λ is shown in Fig. 5. The dependence of δ on λ is evidently non-linear. The cell-free layer decreases at high values of the viscosity contrast after reaching a maximum close to TT-to-TU transition. The existence of cell-free boundary layers is also confirmed by looking at the steady mass density profiles, averaged along the x direction, which are reported in Fig. 6 for two values of λ.

This effect also appears when considering the corresponding steady velocity profiles, averaged along the flow direction, which are shown in Fig. 7. It can be seen that the lack of vesicles, filled with a heavier fluid, produces lower values of mass density close to the walls. The effective shear rate at the center is smaller than the imposed shear rate, while it is larger close to the walls. The observed behavior can be related to the interplay between the reduction of the tilt angle in the TT regime, which favors the packing of vesicles in the channel, and the reduction of the lift force with increasing viscosity contrast.[27]

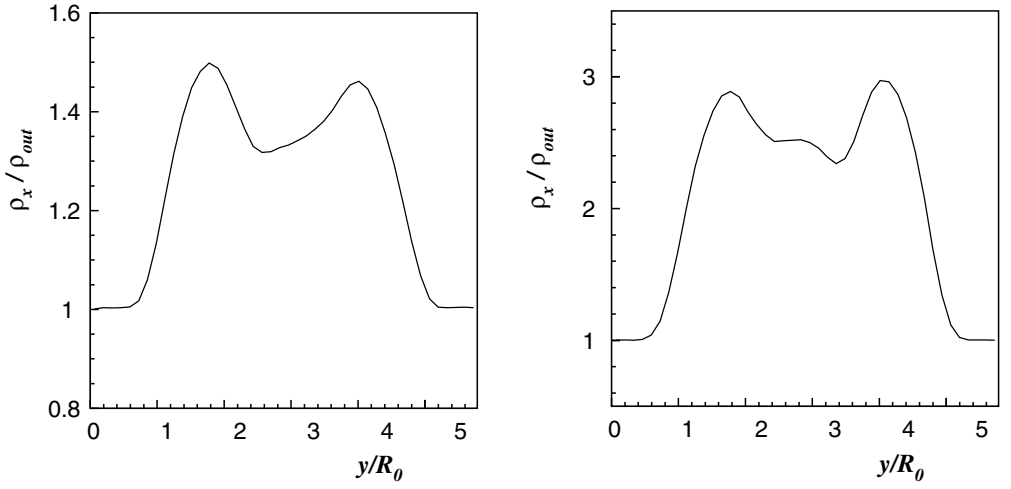

Fig. 6. The ratio of the mass density ρ_x, averaged along the flow direction x, to the solvent mass density ρ_{out} is plotted across the channel for reduced shear rate $\gamma^* = 2.0$, reduced area $A^* = 0.8$, concentration $\phi = 0.28$, and viscosity contrasts $\lambda = 2.0$ (left), 5.0 (right).

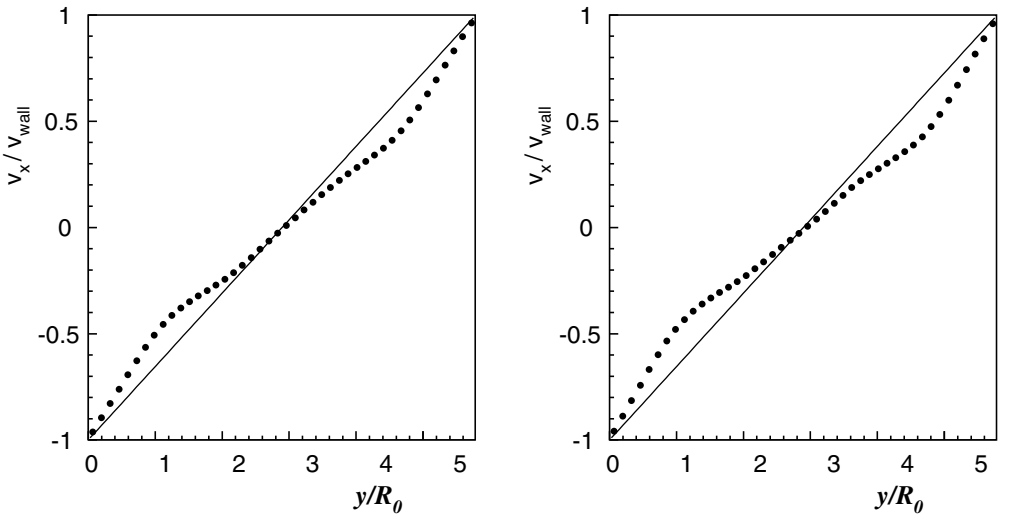

Fig. 7. The stationary velocity profile averaged along the channel is plotted across the channel for reduced shear rate $\gamma^* = 2.0$, reduced area $A^* = 0.8$, concentration $\phi = 0.28$, and viscosity contrasts $\lambda = 2.0$ (left), 5.0 (right). The full line shows the imposed shear rate profile.

4. Summary and Conclusions

We have studied the rheological properties of dilute and semi-dilute vesicle suspensions in wall-bounded shear flow in two dimensions. We find that the intrinsic viscosity is an increasing function of the viscosity contrast. As pointed out in Ref. [12], two main mechanisms should be relevant for the dependence of η_I on λ: Shape fluctuations lead to energy dissipation that increases η_I, while alignment with the flow direction causes a decrease of η_I with increasing λ. Our model, differently from the theory [4,5] and other simulations, [6,7,8,9,10] includes thermal membrane undulations as well as thermal noise in the fluid. The former effect is known to be relevant for the internal dynamics [31,32] and the interaction between vesicles, [33] while the latter contribution induces Brownian diffusion of vesicles across the channel. This implies that a vesicle suspension with Brownian motion can never attain the state of a regular array of vesicles arranged periodically along the centerline of the channel, which is found as a state of minimum dissipation in simulations without thermal noise. [9] A rough estimate of the importance of thermal effects can be given considering

the rotational Peclet number $Pe = \eta_{out}\dot{\gamma}R_0^2/(k_BT)$, which is $Pe = 12.0$ in our study. In the case of a three-dimensional model of vesicles, it was found that thermal fluctuations cannot be neglected for rotational Peclet numbers as large as $Pe = 1200$.[34] More work is in progress to elucidate the role of noise in the observed behavior of the intrinsic viscosity. Moreover, the formation of depletion layers next to the walls is observed for concentrated suspensions: their width increases with the viscosity contrast in the TT regime and then diminishes when entering the TU phase.

In two dimensions, vesicles, capsules and red blood cells cannot be distinguished, because shear elasticity has no analog in two dimensions. Indeed, simulations in two dimensions have been employed to study the behavior of suspensions of red blood cells in microcapillary flows.[35,36] However, as far as the detailed dynamics of individual soft particles and its effects on the suspension viscosity is concerned, the two-dimensional model more resembles fluid vesicles — exactly because of the absence of shear elasticity in two dimensions. In order to elucidate the different behavior of vesicle and cell suspensions, simulations in three dimensions are therefore essential.[37,38,39]

References

1. Vlahovska PM, Podgorski T, Misbah C. Vesicles and red blood cells: from individual dynamics to rheology. *C. R. Physique* 2009; **10**:775.
2. Fedosov DA, Noguchi H, Gompper G. Multiscale Modeling of Blood Flow: From Single Cells to Blood Rheology. *Biomech. Model. Mechanobiol.* 2014; **13**:239.
3. Abreu D, Levant M, Steinberg V, Seifert U. Fluid vesicles in flow. *Adv. Colloid Interface Sci.* 2014; **208**:129.
4. Danker G, Misbah C. Rheology of a dilute suspension of vesicles. *Phys. Rev. Lett.* 2007; **98**:088104.
5. Danker G, Biben T, Podgorski T, Verdier C, Misbah C. Dynamics and rheology of a dilute suspension of vesicles: Higher-order theory. *Phys. Rev. E* 2007; **76**:041905.
6. Ghigliotti G, Biben T, Misbah C. Rheology of a dilute two-dimensional suspension of vesicles. *J. Fluid Mech.* 2010; **653**:489.
7. Rahimian A, Veerapaneni SK, Biros G, Dynamic simulation of locally inextensible vesicles suspended in an arbitrary two-dimensional domain, a boundary integral method. *J. Comput. Phys.* 2010; **229**:6466.
8. Zhao H, Shaqfeh E. The dynamics of a non-dilute vesicle suspension in a simple shear flow. *J. Fluid Mech.* 2013; **725**:709.
9. Thiebaud M, Misbah C. Rheology of a vesicle suspension with finite concentration: A numerical study. *Phys. Rev. E* 2013; **88**:062707.
10. Kaoui B, Jonk RJW, Harting J. Interplay between microdynamics and macrorheology in vesicle suspensions. *Soft Matter* 2014; **10**:4735.
11. Vitkova V, Mader MA, Polack B, Misbah C, Podgorski T. Micro-macro link in rheology of erythrocyte and vesicle suspensions. *Biophys. J.* 2008; **95**:L33.
12. Kantsler V, Segre E, Steinberg V. Dynamics of interacting vesicles and rheology of vesicle suspension in shear flow. *EPL* 2008; **82**:58005.
13. Lamura A, Gompper G. Dynamics and rheology of vesicle suspensions in wall-bounded shear flow. *EPL* 2013; **102**:28004.
14. Malevanets A, Kapral R. Mesoscopic model for solvent dynamics. *J. Chem. Phys.* 1999; **110**:8605.
15. Kapral R. Multiparticle Collision Dynamics: Simulation of Complex Systems on Mesoscales. *Adv. Chem. Phys.* 2008; **140**:89.
16. Gompper G, Ihle T, Kroll DM, Winkler RG. Multi-Particle Collision Dynamics: A Particle-Based Mesoscale Simulation Approach to the Hydrodynamics of Complex Fluids. *Adv. Polym. Sci.* 2009; **221**:1.
17. Kikuchi N, Pooley CM, Ryder JF, Yeomans JM. Transport coefficients of a mesoscopicfluid dynamics model. *J. Chem. Phys.* 2003; **119**:6388.
18. Yeomans JM. Mesoscale simulations: Lattice Boltzmann and particle algorithms. *Physica A* 2006; **369**:159.
19. Noguchi H, Kikuchi N, Gompper G. Particle-based mesoscale hydrodynamic techniques. *Europhys. Lett.* 2007; **78**:10005.
20. Götze IO, Noguchi H, Gompper G. Relevance of angular momentum conservation in mesoscale hydrodynamics simulations. *Phys. Rev. E* 2007; **76**:046705.
21. Allahyarov A, Gompper G. Mesoscopic solvent simulations: Multiparticle-collision dynamics of three-dimensional flows. *Phys. Rev. E* 2002; **66**:036702.
22. Noguchi H, Gompper G. Transport coefficients of off-lattice mesoscale-hydrodynamics simulation techniques. *Phys. Rev. E* 2008; **78**:016706.
23. Mewis J, Wagner NJ. *Colloidal suspension rheology*, Cambridge: Cambridge University Press; 2012.
24. Lamura A, Gompper G, Ihle T, Kroll DM. Multi-particle collision dynamics: Flow around a circular and a square cylinder. *Europhys. Lett.* 2001; **56**:319.
25. Finken R, Lamura A, Seifert U, Gompper G. Two-dimensional fluctuating vesicles in linear shear flow. *Eur. Phys. J. E* 2008; **25**:309.
26. Allen MP, Tildesley DJ. *Computer simulation of liquids*. Oxford: Clarendon Press; 1987.
27. Messlinger S, Schmidt B, Noguchi H, Gompper G. Dynamical regimes and hydrodynamic lift of viscous vesicles under shear. *Phys. Rev. E* 2009; **80**:011901.
28. Belzons M, Blanc R, Bouillot JL, Camoin C. Viscosity of a dilute two-dimensional suspension of spheres. *C. R. Acad. Sci., Paris II* 1981; **292**:939.
29. Keller SR, Skalak R. Motion of a tank-treading ellipsoidal particle in a shear flow. *J. Fluid. Mech.* 1982; **120**:27.
30. Fåhraeus R, Lindqvist T. The viscosity of the blood in narrow capillary tubes. *Am. J. Phys.* 1931; **96**:562.
31. Levant M, Steinberg V. Amplification of thermal noise by vesicle dynamics. *Phys. Rev. Lett.* 2012; **109**:268103.
32. Abreu D, Seifert U. Effect of thermal noise on vesicles and capsules in shear flow. *Phys. Rev. E* 2012; **86**:010902.
33. Helfrich W. Steric Interaction of Fluid Membranes in Multilayer Systems. *Z. Naturforsch.* 1978; **33a**:305.
34. Noguchi H, Gompper G. Dynamics of fluid vesicles in shear flow: effect of membrane viscosity and thermal fluctuations. *Phys. Rev. E* 2005; **72**:011901.
35. Freund JB. Leukocyte margination in a model microvessel. *Phys. Fluids* 2007; **19**:023301.
36. Fedosov DA, Fornleitner J, Gompper G. Margination of White Blood Cells in Microcapillary Flow. *Phys. Rev. Lett.* (2012); **108**:028104.

37. Fedosov DA, Pan W, Caswell B, Gompper G, Karniadakis GE. Predicting blood rheology in silico. *Proc. Natl. Acad. Sci. USA* 2011; **108**:11772.
38. Gross M, Krüger T, Varnik F. Rheology of dense suspensions of elastic capsules: normal stresses, yield stress, jamming and confinement effects. *Soft Matter* 2014; **10**:4360.
39. Fedosov DA, Peltomäki M, Gompper G. Deformation and Dynamics of Red Blood Cells in Flow through Cylindrical Microchannels. *Soft Matter* 2014; **10**:4258.